European Journal of Mechanics / A Solids 109 (2025) 105452

Contents lists available at ScienceDirect

European Journal of Mechanics / A Solids

journal homepage: www.elsevier.com/locate/ejmsol

Full Length Article

Multiphysics analysis of mechanical responses in micro-reactors under varied operating conditions

M. Anjum [a], T. Gibson [b], G.T. Craven [b], S. Tretiak [b], A. Abdelkefi [a,*]

[a] Department of Mechanical and Aerospace Engineering, New Mexico State University, Las Cruces, NM, 88003, USA
[b] Los Alamos National Laboratory, NM, 87545, USA

ARTICLE INFO

Keywords:
Micro-reactors
Multiphysics modeling
Thermal loading
Mechanical loading
Modal analysis
Resonance

ABSTRACT

Micro-reactors are a promising alternative for power production applications where traditional methods may not be feasible (e.g., space missions). Their design requires critical selection of materials, especially for moderator and fuel, to ensure long-term operation and optimal performance. This research focuses on developing computational analysis models for micro-reactors, aiming to explore their structural behavior under thermal and mechanical loadings. The micro-reactor model is based on the Zero Energy Breeder Reactor Assembly (Zebra) Kilowatt (kW) reactor design conceptualized at Los Alamos National Laboratory. This study investigates the thermal and mechanical responses of three distinct reactor models considering factors, such as boundary conditions, material properties, and thermal-mechanical loading. In this study, Beryllium Oxide (BeO), Beryllium (Be), Aluminum Oxide (Al_2O_3), and Magnesium Oxide (MgO) are chosen as materials for the reflector. Yttrium Hydride (YH) and Zirconium Hydride (ZH) are chosen as moderators. Uranium Nitride (UN) and Uranium Molybdenum (UMo) are chosen as reactor fuel materials. The thermal analysis predicts the deformation due to the thermal expansion within the reactor under steady operating conditions at 25 kW_{th}, mimicking the maximum rated power of the Zebra kW design. The mechanical study simulates the system's response to forced vibration loads applied along the cooling channels, matching the natural frequency of the system. The results from both analyses show that Beryllium Oxide, Yttrium Hydride, and Uranium Nitride demonstrate the most optimal stress distribution in the system compared to other configurations investigated here. The results of this study can be developed into datasets to facilitate future machine learning studies, enabling the prediction of mechanical and thermal responses for micro-reactors.

1. Introduction

Space exploration has been a primary interest of developed nations for more than 50 years. In the past few decades, unmanned missions have been successfully conducted on the surface of our neighboring planet Mars. One of the key challenges for these missions is the ability to power the equipment for a sustained period, in order to support these long-term missions and obtain sufficient data. Solar power is one of the solutions currently employed in space missions, however the source is unreliable and cannot be actively used without a storage mechanism, i.e. batteries. Nuclear power offers an alternative to solar power, which does not have the above-mentioned shortcomings. The National Aeronautics and Space Administration (NASA) has been using the concept of micro-reactors for missions to deep space where solar power is not available (McClure et al., 2020). These lightweight reactors can provide power from 100 W (electric) to about 10 kW (electric). Research is ongoing to further develop this technology and increase the power output of these systems, while keeping the compactness of the overall design. Micro-reactors also provide an encouraging avenue to potentially replace the reliance on fossil fuels for domestic power generation (Zohuri, 2021). These systems can be easily integrated into micro-grids for small scale power generation, due to their simple layout and fast installation (Testoni et al., 2021). The zero carbon emissions along with long refueling intervals, low maintenance, and ease of relocation makes them a prime candidate. However, additional improvement is required to justify the cost associated with materials, manufacturing and to make the power production cost competitive to fossil fuels (Black et al., 2023; Gabbar et al., 2020).

Despite the drawbacks inherent in micro-reactors for domestic power production, they continue to be the leading potential technology for off

* Corresponding author.
E-mail address: abdu@nmsu.edu (A. Abdelkefi).

https://doi.org/10.1016/j.euromechsol.2024.105452
Received 6 February 2024; Received in revised form 6 August 2024; Accepted 17 September 2024
Available online 18 September 2024

planet power production. An essential challenge for this application is to increase the lifespan of the system for sustained long-term operation. In contrast to other power generating systems, a nuclear reactor is quiet in its operation and essentially a sophisticated heat exchanger by design, whereby the heat is generated by the fission reaction of the nuclear fuel. In most large-scale reactors, the moderator is in a liquid state and the fuel is packed in the form of pallets in fuel rods. This design approach is not feasible for compact micro-reactor systems that need to be transported and operated in outer space, especially in a scenario where occasional maintenance is infeasible. Hence for micro-reactors, a key design characteristic is the use of solid moderator and fuel materials. For this purpose, Yttrium Hydride is the moderator of choice (Vogel et al., 2021) and the High Assay Low-Enriched Uranium (HALEU) is proposed as the fuel (Carlson et al., 2022). However, controlling the hydrogen loss for such materials is still a challenge in reactor design (Mehta et al., 2019). In regards to mechanical failure for a solid structure, stress plays the primary role. With the absence of any moving components in a nuclear reactor, the main contributor towards stresses is the high temperature reactor core and the high-pressure coolant flow in the cooling channels. Selection of the optimal materials in reactor design is of the utmost important, as it will ensure the robust reactor performance and longevity of operation.

Experimental design analysis is currently infeasible due to the cost and complexity of manufacturing a prototype, however, progress is being made towards development of test facilities for nuclear micro-reactors (Sabharwall et al., 2023). Researchers have also employed coupled numerical codes to predict the response of various reactors' designs during their operation and predict the operating lifespan. Based on the employed numerical code, performance metrics, such as the effect of material selection, reactor thermal profile, stress and strain concentration, reactivity, burnup and hydrogen diffusion can be studied in a combined multiphysics simulation.

Numerical studies have been performed to study the structure response of various novel reactor designs and to analyze their performance metrics. Im et al. (2023) developed a multiphysics framework based on OpenFOAM to study the 2-D thermal expansion of the heat pipes in a heat pipe cooled micro reactor (HPR) under steady-state conditions. Matthews et al. (2021) performed 2-D finite element based simulation using the DireWolf multiphysics code based on the MOOSE framework. Their code was able to simulate the neutron energy fluxes, power density, and temperature profile of a 2-D reactor core under steady-state conditions. Several other studies have been performed including the analysis of reactor heat pipe failure and thermal expansion using the MAMMOTH framework (Hu et al., 2019), simulation of a gas-cooled micro-reactor and its failure under insufficient coolant flow (Stauff et al., 2022), simulation of thermal performance of a nuclear micro-reactor test facility using MOOSE&SAM framework (Zhou et al., 2021). Sun et al. employed a 3-D Finite Element Model (FEM) for a large-scale reactor shell to understand the crack propagation at the reactor wall under thermo-mechanical coupling (Sun et al., 2017). To understand the negative reactivity feedback in their reactor design, Xiao et al. (2022) simulated the thermal expansion of fuel materials using a finite element method (FEM) based simulation model. They also analyzed the reactor design performance under the failure of cooling channels and identified it to be well outside the realm of catastrophic failure (Xiao et al., 2022). Similarly, studies have been conducted to understand the vibration characteristics of reactors' designs for which a significant contribution is identified to be flow-induced vibration (Marcum et al., 2023) and due to the mass distribution in a reactor design (Fan et al., 2023).

Currently, Los Alamos National Laboratory (LANL) has been conducting research on solid-state micro-reactor and their proposed Zero Energy Breeder Reactor Assembly (Zebra) (Mehta et al., 2024) and Open Pool Australian Lightwater (OPAL) (Mehta and Rao, 2022) reactor designs, which show promising results in terms of power output. The Zebra design is predicted to have a thermal output of 25 kW–50 kW. This compact cylindrical design stands at 70 cm in height with a diameter of 45 cm. In the proposed design, 24 cooling channels are distributed evenly along the periphery of the reactor. The moderator material was chosen to be Yttrium Hydride with Beryllium Oxide and Beryllium metal as the reflector material. The proposed design used High Assay Low Enriched Uranium as the fuel material. The original study focused on the thermal performance of the reactor and its performance under insufficient coolant flow (Mehta et al., 2024). As established earlier, failure may occur due to the stresses generated by material expansion under high temperatures and forces due to the high-pressure coolant flow in the channels. High fidelity computational models can be developed to understand the behavior of reactor designs under various mechanical and thermal loading scenarios. A thermo-mechanical multiphysics model will enable researchers to understand the influence of material properties, thermal loading on subsequent response of the reactor. This will also allow the prediction of reactor failure under set operating condition, especially due to the influence of mechanical loading and possible resonance behavior. To better understand the structural responses and performance of micro-reactors under varied operating conditions, here we consider three different micro-reactor designs based on the Zebra kW reactor, under thermal and mechanical loadings. The mechanical response is analyzed for various boundary conditions, moderator, fuel and reflector material, and thermal-mechanical loading. In this study, Beryllium Oxide (BeO), Beryllium (Be), Aluminum Oxide (Al_2O_3), and Magnesium Oxide (MgO) are chosen as materials for the reflector, while Yttrium Hydride (YH) and Zirconium Hydride (ZH) are selected as moderators, and Uranium Nitride and Uranium Molybdenum (UMo) are chosen as reactor fuel materials. The rest of this article is composed as follows: Section 2 focuses on the problem formulations and designs' specifications. Section 3 discusses the computational model. In Section 4, we present our findings. We conclude our study in Section 5.

2. Problem formulation: reactor design and system's modeling

The micro-reactor design is based on the Zebra kW class reactor, conceptualized at LANL. In the original study, the reactor model was comprised of Uranium as the fuel material, stacked between plates of Hydride moderator, as shown in Fig. 1(a) (Mehta et al., 2024). For this study, the original design is modified to a simpler configuration, whilst keeping the original dimensions of the Zebra kW reactor. This approach allows us to analyze the distribution of stresses and the temperature distribution inside the reactor, and make effective design changes, to keep the aforementioned parameters under permissible limits and maximize the reactor's operating lifespan. For all designs, the area encompassing the fuel and moderator is kept the same. These results are simulated for a constant output power of the reactor in all three designs. The major difference in the three designs is the number of cooling channels, as apparent in Fig. 1(b) and (c). Starting from such a simple model allows the development of our computational model and the establishment of an accurate solver technique within the COMSOL software, to capture the underlying physics.

Design 3 of the reactor closely matches the original model of the Zebra kW class reactor, as presented in Fig. 2. For this study, a transient heat transfer analysis, in conjunction with a mechanical analysis study is

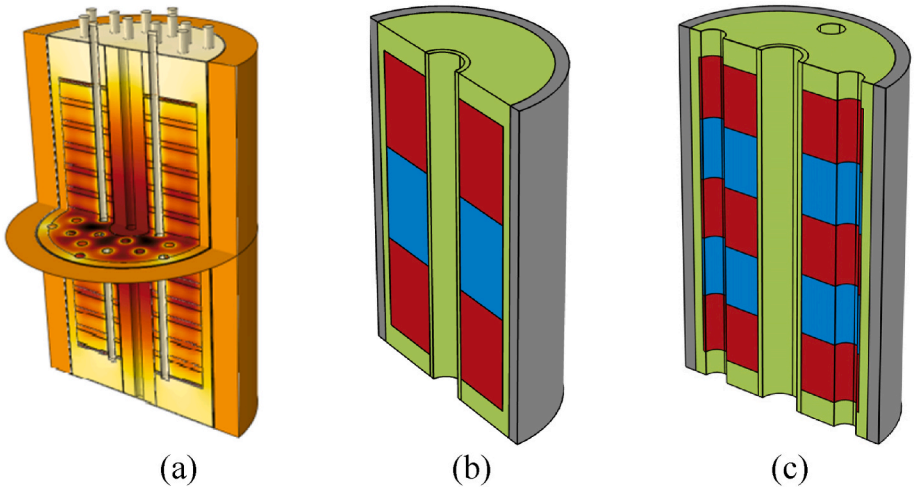

Fig. 1. Reactor designs: (a) original Zebra kW model, (b) design 1: consists of a single cooling channel, single moderator plate (blue) stacked between two fuel plates (red), an outer reflector (grey) and inner reflector (green), and (c) design 2: cooling channel increased to five with three fuel plates (red) stacked with two moderator plates (blue). (For interpretation of the references to colour in this figure legend, the reader is referred to the Web version of this article.)

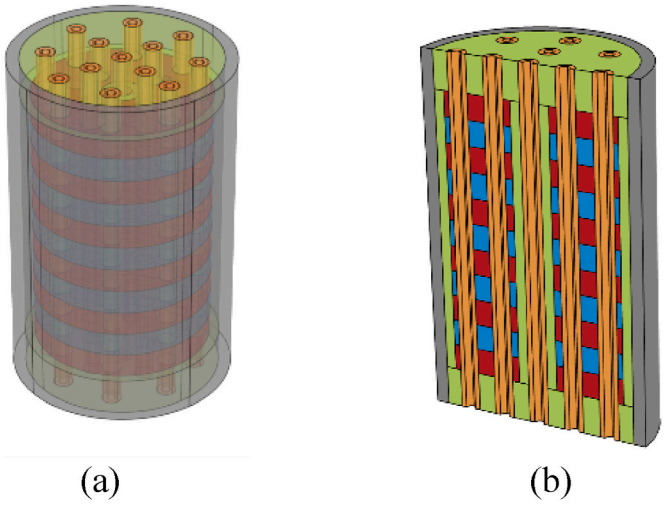

Fig. 2. (a) Design 3: consists of thirteen cooling channels with five moderator plates stacked between six fuel plates, and (b) design 3 cross-section (isometric-view).

conducted on all three designs. These simulation models require the definition of operating conditions, *i.e.*, the thermal and mechanical loadings on the reactor and the respective boundary conditions. The heat flux is based on the original power output of the Zebra kW class reactor, *i.e.*, 25 kW thermal at full power. This is applied to the simulation model as a time varying heat flux generating through the fuel material. For the heat transfer simulation step, the reactor reaches its maximum operating power in 2 h. At that point, coolant flow is introduced into the simulation model and the simulation is continued for another 4-h operating period. Hence, a data set is obtained for a 6-h period of reactor operation, from startup to steady-state operation.

The mechanical loading is introduced in the form of a harmonic force. The coolant is modeled as water at a pressure of 15 MPa and temperature 523 K. The coolant flow velocity is set to 4 m/s to generate an effective convective heat transfer coefficient. Fig. 3(b) presents the time varying harmonic load applied to the reactor simulation model. The corresponding frequency of harmonic load is always matched with the first natural frequency mode of the respective reactor design configuration. The purpose of this approach is to introduce vibratory motion into the system and study the mechanical response of the selected design near resonance. The input force per unit area acts as a shear force at the walls of the cooling channel and the frequency of

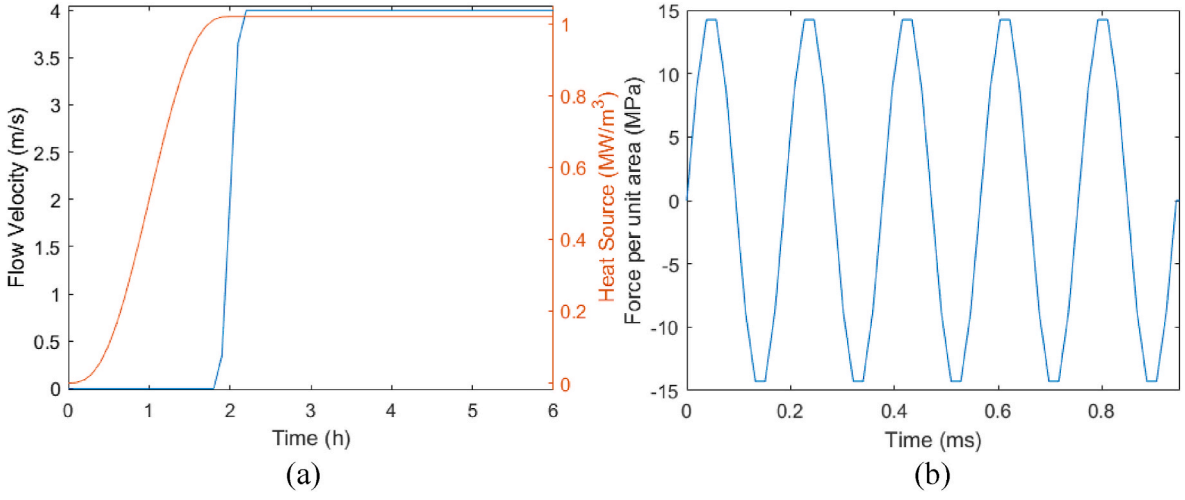

Fig. 3. (a) High pressure coolant flow in reactor coolant channel introduced when the reactor reaches maximum thermal capacity and heat flux variation applied on fuel plates, and (b) harmonic load based on the first natural frequency of the selected design.

Table 1
Material properties.

Materials	Density "ρ" (kg/m^3)	Young's modulus "E" (GPa)	Poisson's ratio "μ"	Heat capacity "C_p" (J/(kg·K))	Thermal expansion coeff. "α" (1/K)	Thermal conductivity "k" (W/(m·K))
	Reflector					
Beryllium metal (Be) (Bauccio, 1994)	1850	287	0.032	420	1.13 x10^{-5}	200
Beryllium Oxide (BeO) (Konings and Stoller, 2020)	3010	332	0.26	1050	8.00 x10^{-6}	250
Aluminum Oxide (Al_2O_3) (Dorogokupets et al., 2016)	3960	370	0.22	1088	2.50 x10^{-6}	18.9
Magnesium Oxide (MgO) (AZoM Magnesia, 2023)	3580	330	0.36	950	1.05 x10^{-5}	60
	Moderator					
Yttrium Hydride (YH) (Hu et al., 2021)	4270	135	0.225	600	1.20 x10^{-5}	40
Zirconium Hydride (ZH) (Araki et al., 2015; Yamanaka et al., 1999)	5624	130	0.34	550	2.70 x10^{-6}	17
	Fuel					
Uranium Molybdenum (UMo) (Phillips et al., 2010)	18000	90	0.39	181	1.67 x10^{-5}	35.4
Uranium Nitride (UN) (Bobkov et al., 2008; Taylor and McMurtry, 1961)	14211	187	0.215	223	8.04 x10^{-6}	17.9

vibration is adjusted according to the natural frequency of design, based on the selected material configuration.

The fuel materials used for this study are based on the original study on the Zebra kW class reactor. Additional fuel and moderator materials are selected based on their performance and importance towards the development and feasibility requirement in design and long-term operation of a micro-reactor (Rao et al., 2020). The materials are used in various combinations for the heat transfer and mechanical analysis studies. The materials used as moderator, fuel, and reflector in the simulation model are shown in Table 1. The material properties are selected based on the requirement of the COMSOL Multiphysics simulation framework (Schenk and Gärtner, 2004). The values of these materials are fixed on the basis of reactor steady-state operating conditions, and the target of maximum temperature inside the reactor, that is about 550 K. The constant material properties greatly simplify the simulation model and significantly reduces the required computational resources.

The boundary conditions studied for the reactor model emulate the installation condition for the reactor and we aim to study how it affects the stresses generated in the system during the reactor operation. The three boundary conditions selected are illustrated in Fig. 4. The variation in boundary conditions brings about a change in natural frequencies and vibratory modes of the system, which changes the system's mechanical response under harmonic loading at a specific frequency.

3. Computational modeling, solver, and convergence analysis

The reactor design and computational models were developed using the COMSOL Multiphysics software (Schenk and Gärtner, 2004). COMSOL provides a simple interface to model multiple physics independently and simulate the overall model in a combined manner. For the designs of the micro-reactor systems, COMSOL's heat transfer and structure module are used in parallel and modeled as a multiphysics simulation. The heat transfer model is solved using the 3D unsteady heat transfer equation, as shown in equation (1). The heat transfer and the structure mechanics model are solved in a segregated manner.

$$\rho C_p \frac{\partial T}{\partial t} + \rho C_p \cdot \mathbf{v} \cdot \nabla T + \nabla \cdot \boldsymbol{q} = Q \tag{1}$$

where ρ is material density, C_p is the specific heat at constant pressure, T represents the temperature field, t is time, $\boldsymbol{q}$ denotes the heat flux, Q represents the heat source, and $\mathbf{v}$ is the velocity.

The heat transfer model uses the PARallel DIrect SOlver (PARDISO) algorithm to solve the unsteady heat transfer equation. PARDISO incorporates the system in a general form of matrix $Ax = b$. The algorithm for PARDISO uses the Basic Linear Algebra Subprograms (BLAS) update technique, along with a combination of super-node and pipelining parallelism techniques. This improves numerical factorization in parallel and sequential solutions. The solver computes the solution in a segregated manner whereby the solution from the heat transfer step is used an input to the solid mechanics solution step. Detailed description and execution of the PARDISO can be found in these references (Schenk and Gärtner, 2004; COMSOL).

The linear solid mechanics model is solved using the MUltifrontal Massively Parallel Sparse direct Solver (MUMPS). The MUMPS solver like PARDISO incorporates the system in a general form of matrix. It permutes the matrix columns using various preordering algorithms which minimizes the fill-in (Amestoy et al., 2000). Convergence is monitored at each time step and tolerance is set to the order of O(10^{-6}) for convergence of heat transfer equation at a single time step. The displacement field for the structure is modeled in COMSOL using the equilibrium equations given by the Newton's second law, as shown in equation (2). The displacement field is obtained during the segregated step, taking the thermal expansion as input from the heat transfer step, to obtain the upgraded displacement field. The simulation model represents a one-way coupling physics, whereby the effects of the heat

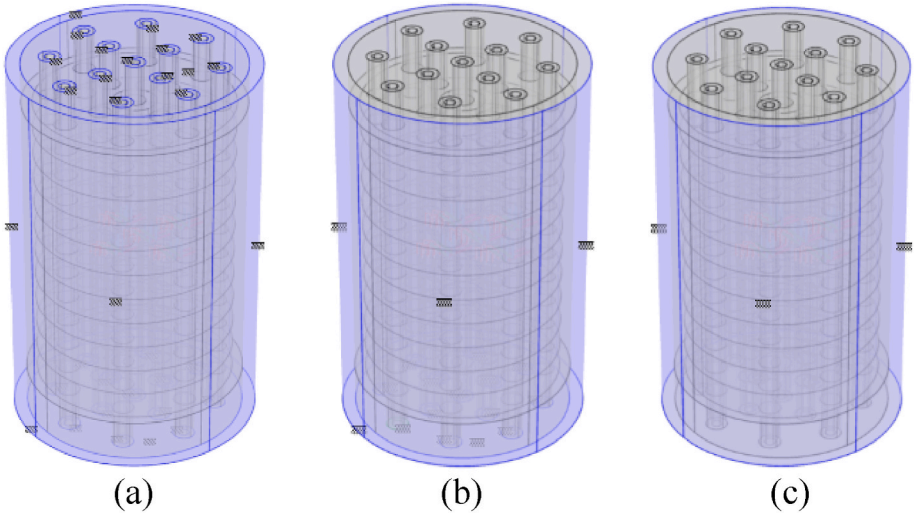

Fig. 4. The boundary conditions studied: (a) all boundaries fixed (A.B.F), where the reactor is constrained from all outer sides against deformation, (b) the outer and bottom boundaries fixed (O.B.F), where deformation is allowed at the top most part of the reactor, and (c) the only outer boundary fixed (O.O.F), where both the top and bottom part of reactor are left unconstrained.

transfer analysis are transferred to the solid mechanics study.

$$\rho\frac{\partial^2\boldsymbol{u}}{\partial t^2}=\nabla\cdot(\mathrm{FS})^T+\boldsymbol{F}_v \tag{2}$$

where $\boldsymbol{u}$ is the displacement field, FS is the first Piola stress tensor, and $\boldsymbol{F}_v$ denotes the applied volume force vector.

For the forced vibration analysis, the COMSOL solver uses the MUMPS direct solving technique to compute the displacement field. The applied volume force vector contains the applied forcing in the three principal directions. For the forced vibration analysis, only a single direction is considered corresponding to the first mode of vibration of reactor design. Due to the same mode shape at first natural frequency for all configurations and boundary conditions, the forcing direction remains constant and only the frequency is changed for the applied harmonic load shown in Fig. 3(b).

For the eigenfrequency model, it solves for the natural frequencies of the system, as shown in equation (3). The direct solver approach works best for simple designs, where mesh refinement is not required and large number of elements are enough for convergence, as the memory requirement is not demanding. Whereas, for complex designs, where convergence is not achieved with a coarse mesh, and mesh refinement is required, the direct approach becomes demanding in terms of memory. Hence, for such cases, iterative solvers are used in the forced vibration analysis study as well, similar to the heat transfer study:

$$-\rho\omega^2\boldsymbol{u}=\nabla\cdot(\mathrm{FS})^T \tag{3}$$

where ω is the natural frequency.

A mesh independence study is further performed to understand the mesh requirement for the simulation models. As shown in Fig. 5, the mesh is kept finer at the regions of stress concentration, notably the cooling channels and the moderator and fuel plates. Switching from design 1 to design 2, only a small increase in the number of elements is observed, in order to aid convergence. For design 3, the number of elements is significantly higher due to the increase in the number of cooling channels, moderator, and fuel plates.

The convergence analysis results from the modal analysis study shows convergence up to five significant figures for all mesh refinements. The accuracy is reduced to the fourth significant figure for

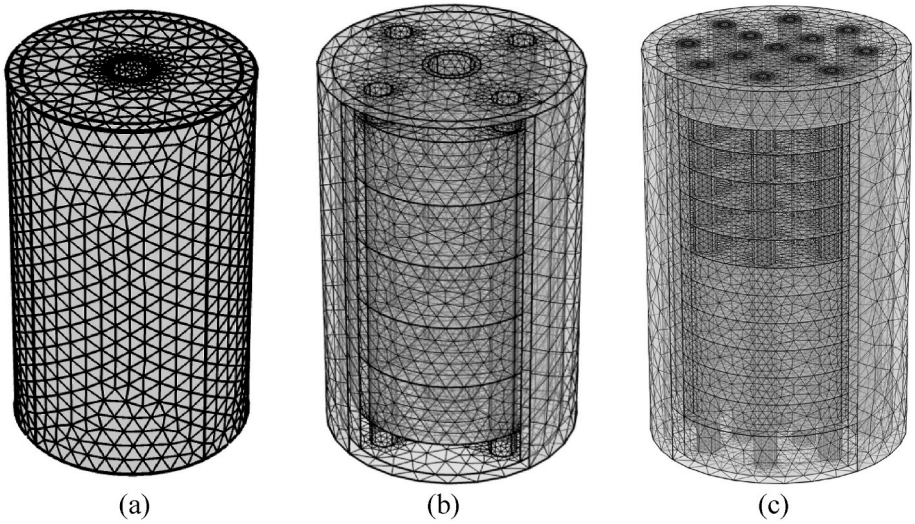

Fig. 5. An unstructured tetrahedral mesh is used to discretize the simulation model: (a) design 1 (finer mesh, 41514 mesh elements), (b) design 2 (finer mesh, 44725 mesh elements), design 3 (finer mesh, 895840 mesh elements).

higher frequency modes. However, the convergence for the modal solver indicates that the error for both meshes is of the order of $O(10^{-15})$, which proves to be sufficient for our study to proceed with the finer mesh, as the preferred mesh of selection.

4. Performance of the reactor under mechanical and thermal loadings

In the first section of this study, the thermal profiles of the reactor designs are investigated, considering various configurations of fuel, moderator and reflector materials. In the second section, eigenfrequency analysis of the three designs is performed to study the mode shapes and natural frequencies of the system. The results from the eigenfrequency analysis are used to setup the harmonic load for the forced vibration study, to understand the reactor design structural response near resonance.

4.1. Influence of thermal loading on various reactor material configurations

The thermal analysis study is conducted for a maximum thermal load of 25 kW_{th} for a steady-state period of 4 h. For comparison, the thermal analysis results with all boundaries fixed (A.B.F) are considered for all three reactor designs, where the outer, top and bottom surfaces are constrained against deformation. For the thermal analysis, the performance parameters considered for analysis are the maximum temperature in the reactor, the maximum temperature difference in the reactor, and the deformation due to the thermal expansion. It can be seen from Fig. 6(a) that the selection of Aluminum Oxide (Al_2O_3) as the reflector material results in a maximum temperature reached in the reactor in all three designs. An increase in reactor's temperature is also seen when the fuel material is switched from Uranium Molybdenum (UMo) to Uranium Nitride (UN). Concerning the maximum temperature difference in the micro-reactor, it follows from the results in Fig. 6(b) that a similar trend is observed as the maximum temperature depicted in Fig. 6(a). Indeed, the maximum temperature difference in the reactor designs appears for the configurations with Aluminum Oxide (Al_2O_3) as a reflector and this difference is highest for design 1. It is also observed that a switch from Uranium to Uranium Nitride as fuel material brings an increase in all three performance parameters. It should be mentioned that the lowest temperature that is estimated inside the reactor is 540 K. The difference in maximum temperature inside the reactor between all configuration of fuel, reflector and moderator material reduces as we move from design 1 to design 2 to design 3, as shown in Fig. 6(b).

As for the deformation, as indicated in Fig. 6(c), it is clear that the consideration of Uranium Nitride (UN) as a fuel results in a decrease in the deformation for all three designs under investigation. This is due the lower thermal expansion coefficient of UN compared to the UMo counterpart. As for the reflector and moderator configuration, inspecting Fig. 6(c), it is noted that the smallest maximum deformation values

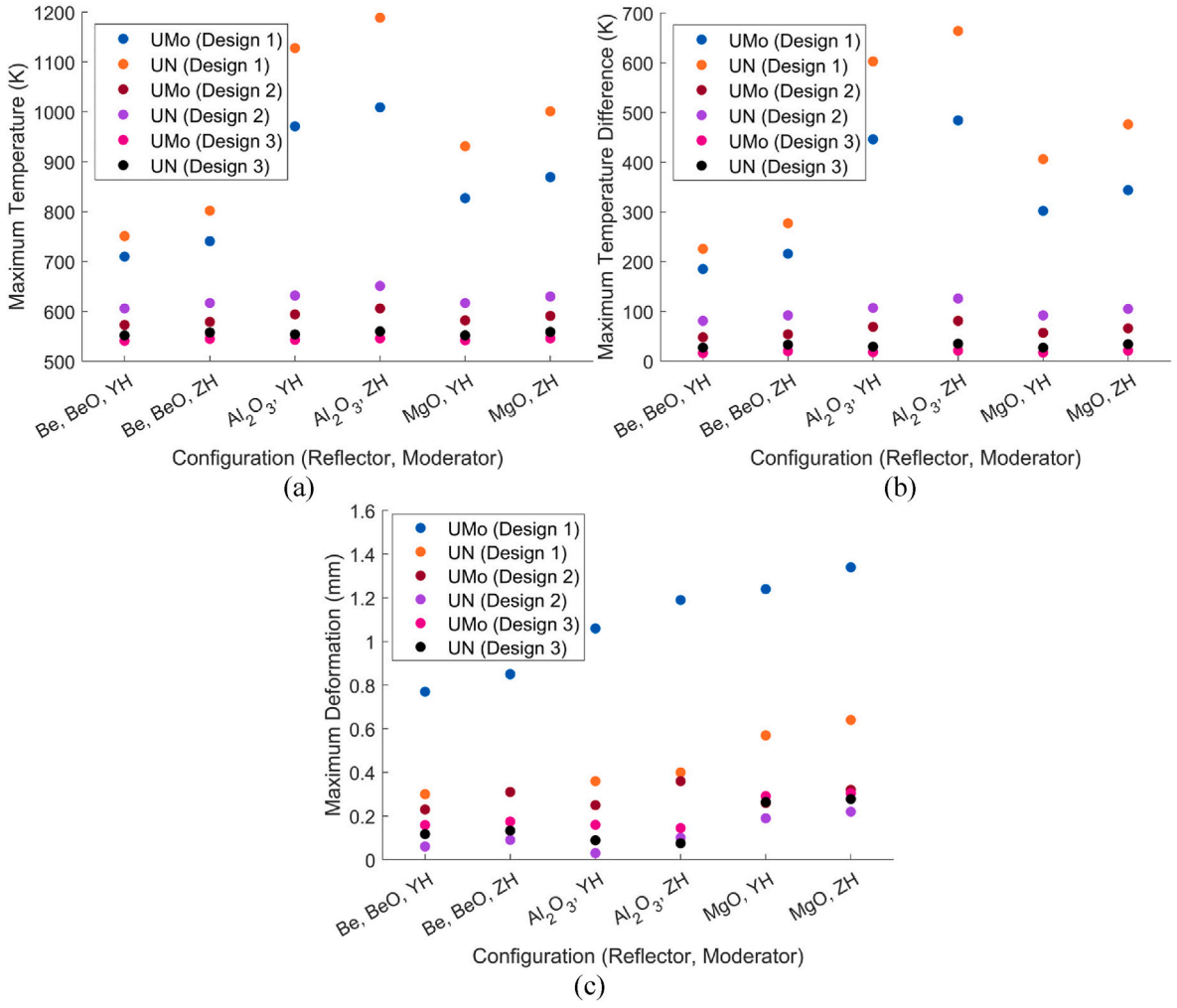

Fig. 6. Summary of thermal analysis results: (a) maximum temperature observed in all three reactors' designs for various fuel and moderator configurations, (b) maximum temperature difference in all three reactors' designs, and (c) maximum deformation due to thermal expansion of reactors' materials in all three reactors' designs.

are generally observed for the Aluminum Oxide (Al_2O_3) or Beryllium Oxide (BeO) as a reflector and Yttrium Hydride (YH) as a moderator. This result may be due to comparatively lower value of thermal expansion coefficient of Al_2O_3, BeO, and YH compared to the other scenarios, as shown in Table 1.

The temperature difference inside the reactor for design 3 is calculated to be a maximum value of 50 K in all six configurations of materials. The behavior for the temperature difference and the maximum temperature in the reactor does not carry over to the deformation inside the reactor system, for all three designs. For design 1, the deformation in the reactor is found to be maximum for the configuration of Al_2O_3 and MgO, as the reflective material, as evident in Fig. 6(c). For these materials, the deformation increases when the moderator material switches from YH to ZH. Furthermore, the effect of replacing the fuel material from UMo to UN is opposite in the case of deformation as compared to the case of temperature differences and the maximum temperature. When analyzing the deformation, it reduces upon switching from UMo to UN fuel, for a specific set of reflector and moderator materials. This behavior stems from the material property of UN as its expansion coefficient is smaller compared to UMo. Therefore, a choice must be considered when deciding between UMo and UN fuels, whether to attain a substantial temperature difference in the reactor or to reduce the temperature difference value, albeit at the expense of heightened deformation and increased stresses imposed on the system.

The results from the thermal analysis study allows for the most effective selection available for fuel, reflector, and moderator materials, whilst considering minimum temperature difference, and minimum deformation due the thermal expansion in the reactor as the performance parameters. It is suggested BeO as the reflective material, YH as the moderator material, and UMo or UN as the fuel material. Analyzing the stress distribution and the temperature distribution in the reactor system for this configuration shows us that the highest temperature achieved inside the reactor system is 540 K and the lowest temperature is 524 K, as seen in Fig. 7(a) and (b). The low temperature is defined by the temperature of the coolant flow in the cooling channels. For design 3, the small difference inside the reactor points towards maximum heat are carried out of the system and high thermal efficiency of the system. The maximum temperature is seen inside the fuel material and the lower temperatures are observed around the cooling channels. Similarly, for the deformation due to the thermal expansion, it is maximum for all fuel

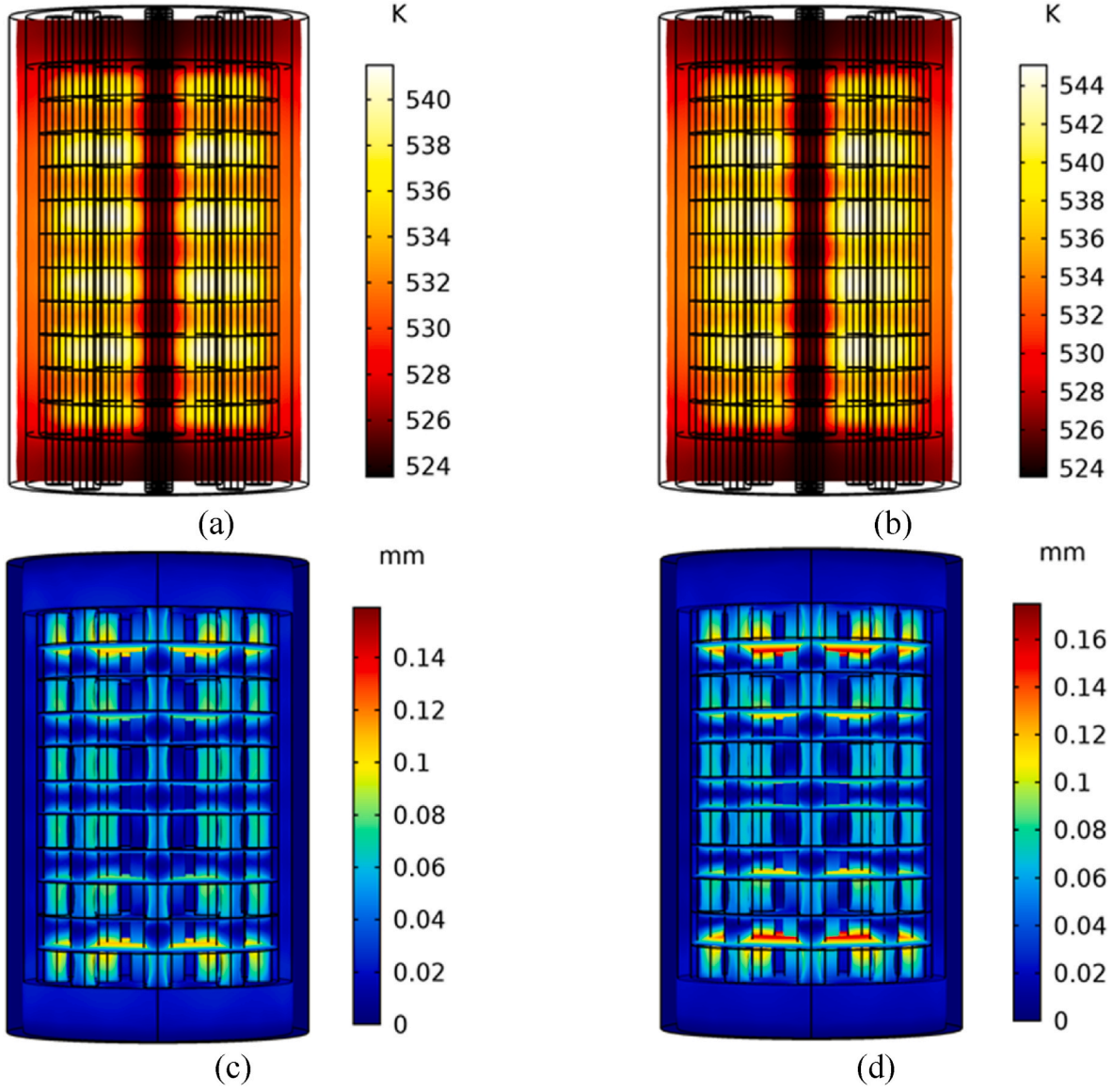

Fig. 7. Temperature distribution (a, b) and deformation due to the thermal expansion (c, d) with all boundaries fixed: (a) Be, BeO, YH, and UMo case, (b) Be, BeO, ZH, and UMo case, (c) Be, BeO, YH, and UMo case, and (d) Be, BeO, ZH, and UMo case.

plates as compared to the moderator and reflector materials. The regions of high stresses are formed where the fuel material is in contact with the reflector and the cooling channels, and these regions are identified to be the stress concentrations where failure would most likely to occur during the operation of the reactor during its lifespan.

Analyzing the effect of boundary conditions, a difference in maximum deformation is observed for the various selected configurations. For this analysis, we focus on design 3, since its thermal profile and deformation behavior are considerably better than the other two designs. As seen from Fig. 8(a) and (b), the highest deformation and stresses are observed for the cases of MgO as reflector material. For all configurations, highest thermal expansion and the resulting deformation is seen in the fuel plates of UMo and UN. The two boundary conditions, outer bottom fixed (O.B.F) and only outer fixed (O.O.F) provide similar results without any significant change in deformation and stress values. A considerable reduction in deformation is observed for all boundaries fixed (A.B.F) condition, for all material configurations. The results also indicate reduced deformations and stresses when UN is selected as fuel over UMo, as previously observed for all three designs. The change in deformation amongst various material configuration is significantly reduced with A.B.F condition, however, the generated stresses do not portray the same behavior with this boundary condition.

From Fig. 8(a), lowest stresses are seen for the configuration with Al_2O_3 as the reflector material and a small increase is observed when switching to Be and BeO as reflector material. The difference is observed to be about 0.5 GPa between the maximum stress observed with Be, BeO and minimum stress observed with Al_2O_3. It is also observed that maximum deformation does not dictate the stress being generated, rather the location of deformation and the respective boundary conditions on the reactor design have a much more prominent effect on stresses. It can be seen from Fig. 8(a) and (b) that deformation is similar in all material configurations with the all-boundaries fixed condition (A.B.F), however the stresses between them are quite dissimilar. By analyzing Fig. 9(a) and (b) and comparing the information with Fig. 8(a) and (b), we can conclude that deformation nearer to the constrained surfaces, such as the top and bottom of the reactor contribute significantly towards the stresses, whereas the deformation at the middle part of the reactor produces lower stresses in comparison. Prominent examples of this are the cases of Al_2O_3, YH, UMo and Al_2O_3, ZH, UMo having maximum deformation in the middle part of the reactor and low stresses. Whereas, the cases of Be, BeO, YH, UMo and Be, BeO, YH, UN have low deformation, but high stresses, due to the location maximum deformation at the bottom of the reactor close to the constrained surface.

For design 2, the behavior of maximum deformation shows similar trends as design 3, as presented in Fig. 10(a) and (b). For most cases, the maximum deformation due to the thermal expansion is observed near the constrained surfaces. In comparison with design 3, the highest expansion was obtained away from the cooling channels and at the fuel plates in design 2. This occurs primarily due to the fewer number of cooling channels present in design 2 and less heat transfer capability, resulting in higher temperature at the fuel and moderator plates. For design 1, maximum deformation is observed in the region surrounding the single cooling channel, as shown in Fig. 11. This highest deformation is seen in the fuel plates primarily due to the high temperature and less heat transfer capability of the design. The deformation due to the thermal expansion is similar to previous designs for all configurations, with MgO experiencing the highest deformation and Be and BeO having the lowest. To note, in all three designs, the highest expansion is seen in either UMo or UN fuel plates, as indicated in Figs. 9–11.

Due to their high heat capacities and low thermal conductivities, Al_2O_3 and MgO act as insulating materials resulting in high temperatures in moderator and fuel plates, which leads to highest thermal expansion in UMo and UN in all designs. The reflector materials Be and BeO exhibit superior thermal properties than MgO and Al_2O_3 resulting in an even distribution of temperatures in the reactor design and lower deformation of fuel plates. For thermal analysis, the choice of boundary condition is not found to be a significant influence on reactor design performance. It only dictates the stresses in the design, which do not change significantly with the switching of boundary conditions.

For design 3, Fig. 12 shows that the magnitude of stress is lowest for the case of only outer fixed boundary (O.O.F), in which the maximum stress inside the system is seen to be around 2 GPa, and the stress is found to be concentrated around the periphery of the cooling channels. As more constraints are introduced into the system, in the form of boundary conditions at the top and bottom of the reactor, the magnitude of stress inside the reactor increases and the distribution of that stress expands from the cooling channels to the outer part of the reactor and into the reflective material. The highest amount of stress is seen to be 2.6 GPa for the boundary conditions where the entirety of the reactor is constrained from the outer, bottom and the top (A.B.F).

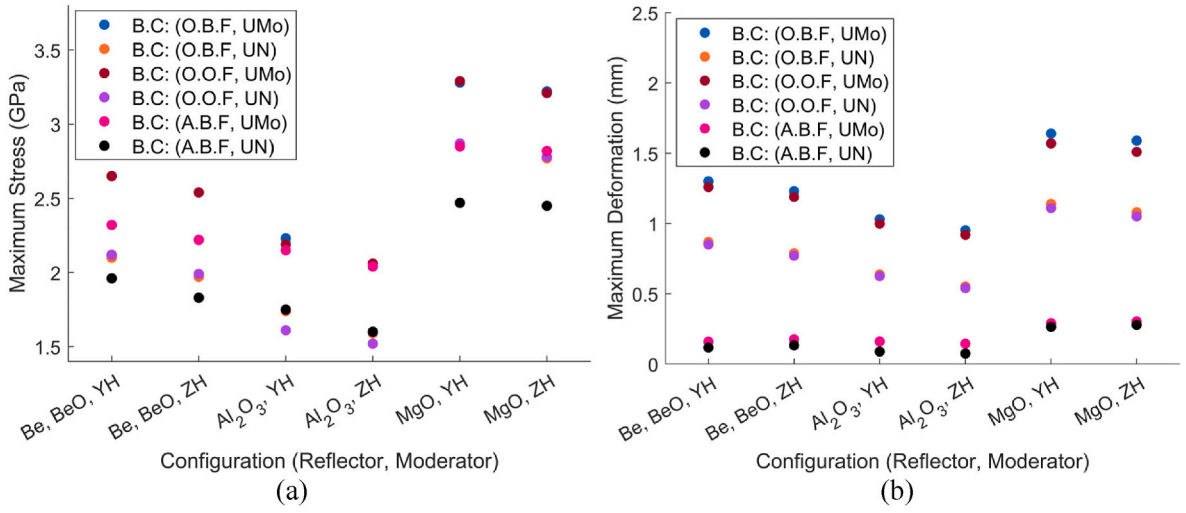

Fig. 8. (a) Maximum stress for each boundary condition (design 3) and (b) maximum deformation for each boundary condition (design 3).

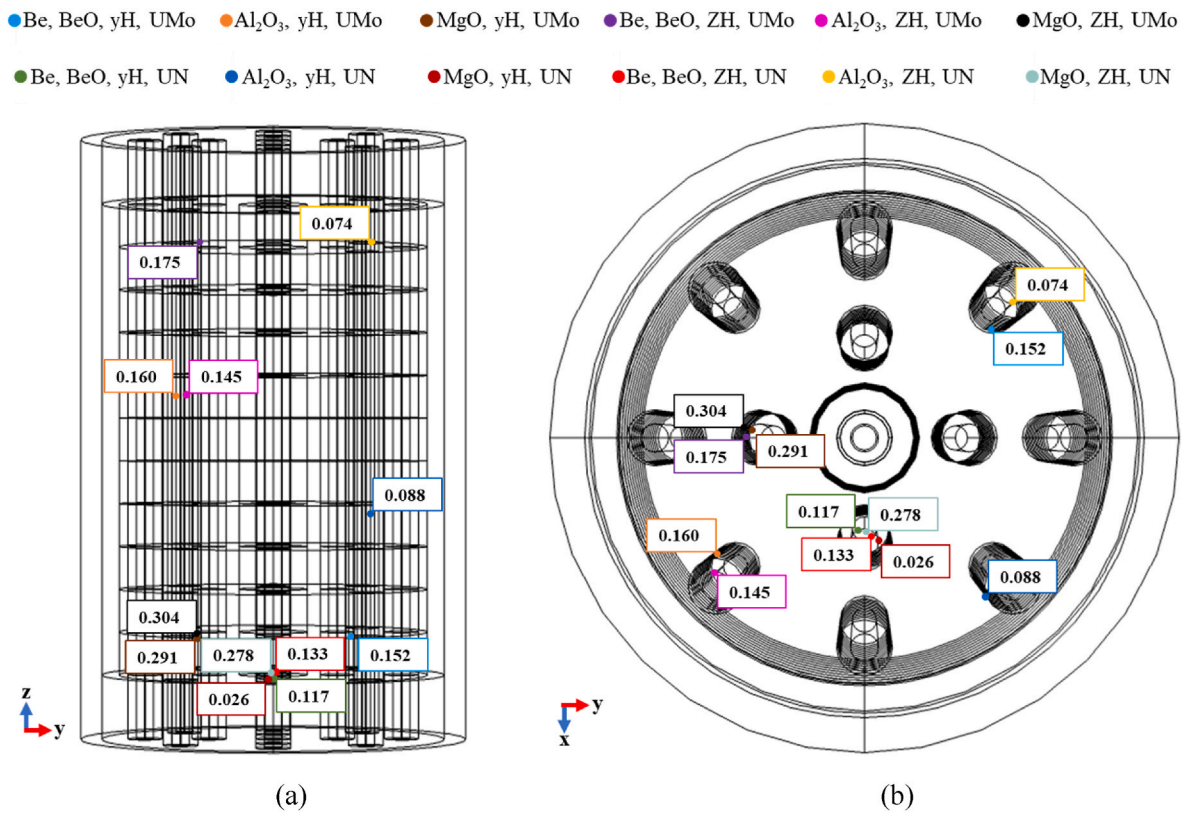

Fig. 9. Locations of maximum deformation (mm) for design 3 with all boundaries fixed (A.B.F): (a) front view (z-y plane), (b) top view (x–y) plane.

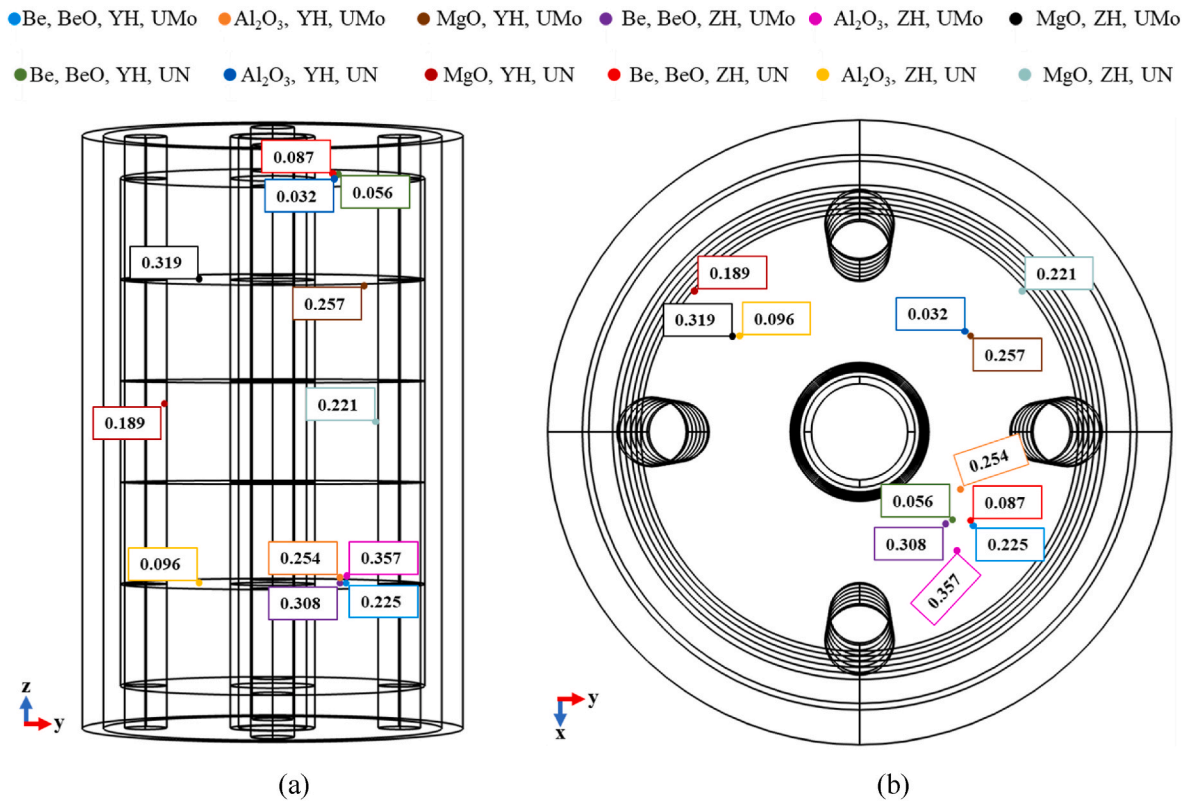

Fig. 10. Locations of maximum deformation (mm) for design 2 with all boundaries fixed (A.B.F): (a) front view (z-y plane), (b) top view (x–y) plane.

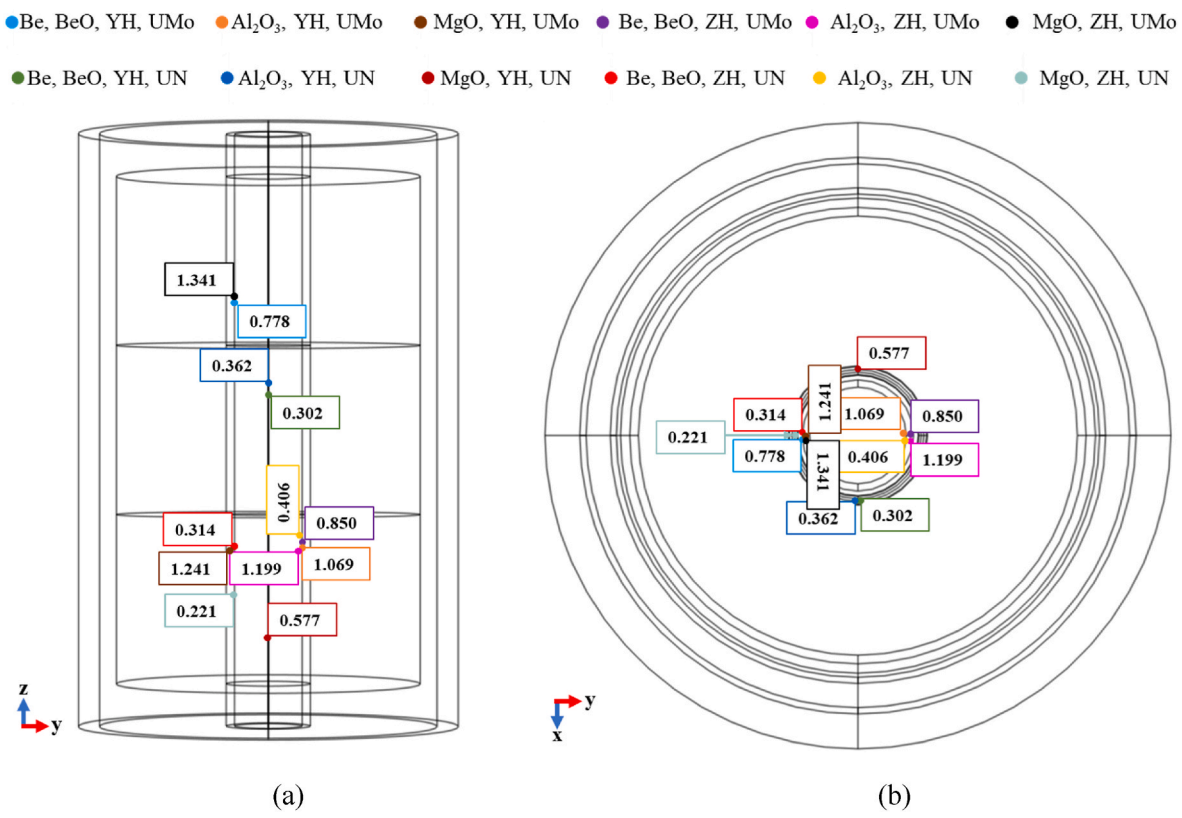

Fig. 11. Locations of maximum deformation (mm) for design 1 with all boundaries fixed (A.B.F): (a) front view (z-y plane), (b) top view (x–y) plane.

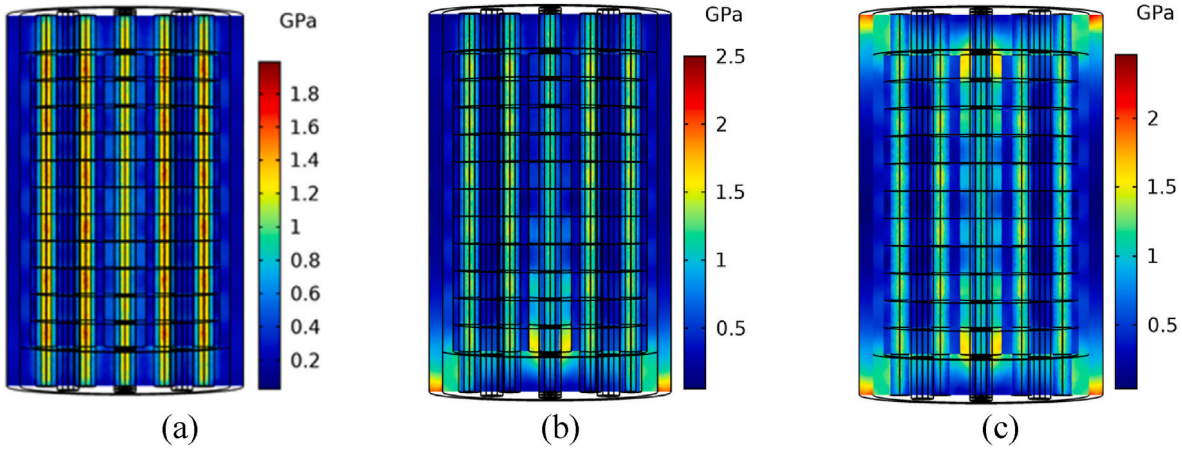

Fig. 12. Stress distribution plots for case of Be, BeO, YH, UMo materials, for design 3, where (a) only outer boundaries fixed (O.O.F), (b) outer bottom boundaries fixed (O.B.F), and (c) all boundaries fixed (A.B.F).

4.2. Mechanical responses of the micro-reactor: influence of the material properties and boundary conditions

4.2.1. Effects of the boundary conditions and material properties on the modal characteristics of the micro-reactor

The first part of mechanical analysis focuses on the natural frequencies and mode shapes of the system and how they change with the boundary conditions and the material properties of the reactor design. This study is conducted only on design 3, as that proved to be much more practical considering the results of the thermal analysis. The fundamental natural frequency for different boundary conditions on the reactor design 3 is then used as input frequency to the harmonic load in the forced vibration analysis.

The simplest mode of vibration for design 3 is found to be the first natural frequency mode of the reactor design. The pattern of deformation remains the same regardless of the change in boundary conditions. As seen in Fig. 13, the first mode of vibration is a vertical deformation along the cooling channels of the reactor. Any such load that may be applied or randomly introduced on the cooling channel, while matching the first natural frequency of the system, can introduce large deformation due to the resonance phenomenon. This could result in a drastic failure for the micro-reactor during its operation. The first natural frequency value is found to be 4266.5 Hz for the case of the outer fixed boundary and this frequency value increased as the reactor model is constrained form the top and bottom wall.

For design 3, Fig. 14 shows the frequency values for the first three non-symmetric modes of vibrations for all configurations. The highest frequencies are seen for the all boundaries fixed condition (A.B.F). In

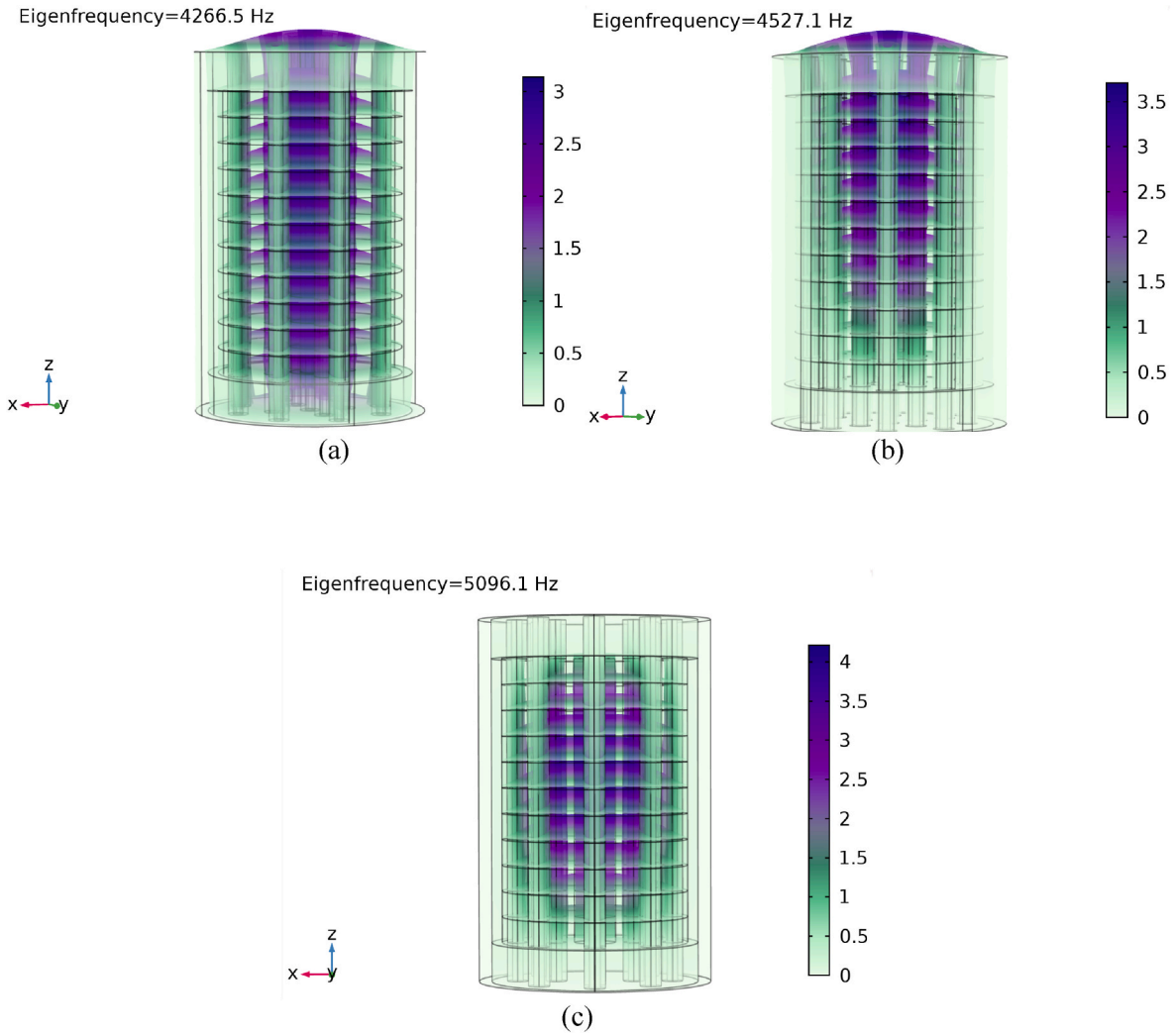

Fig. 13. Natural frequencies: (a) first mode shape (only outer fixed), (b) first mode shape (outer bottom fixed), and (c) first mode shape (all boundaries fixed).

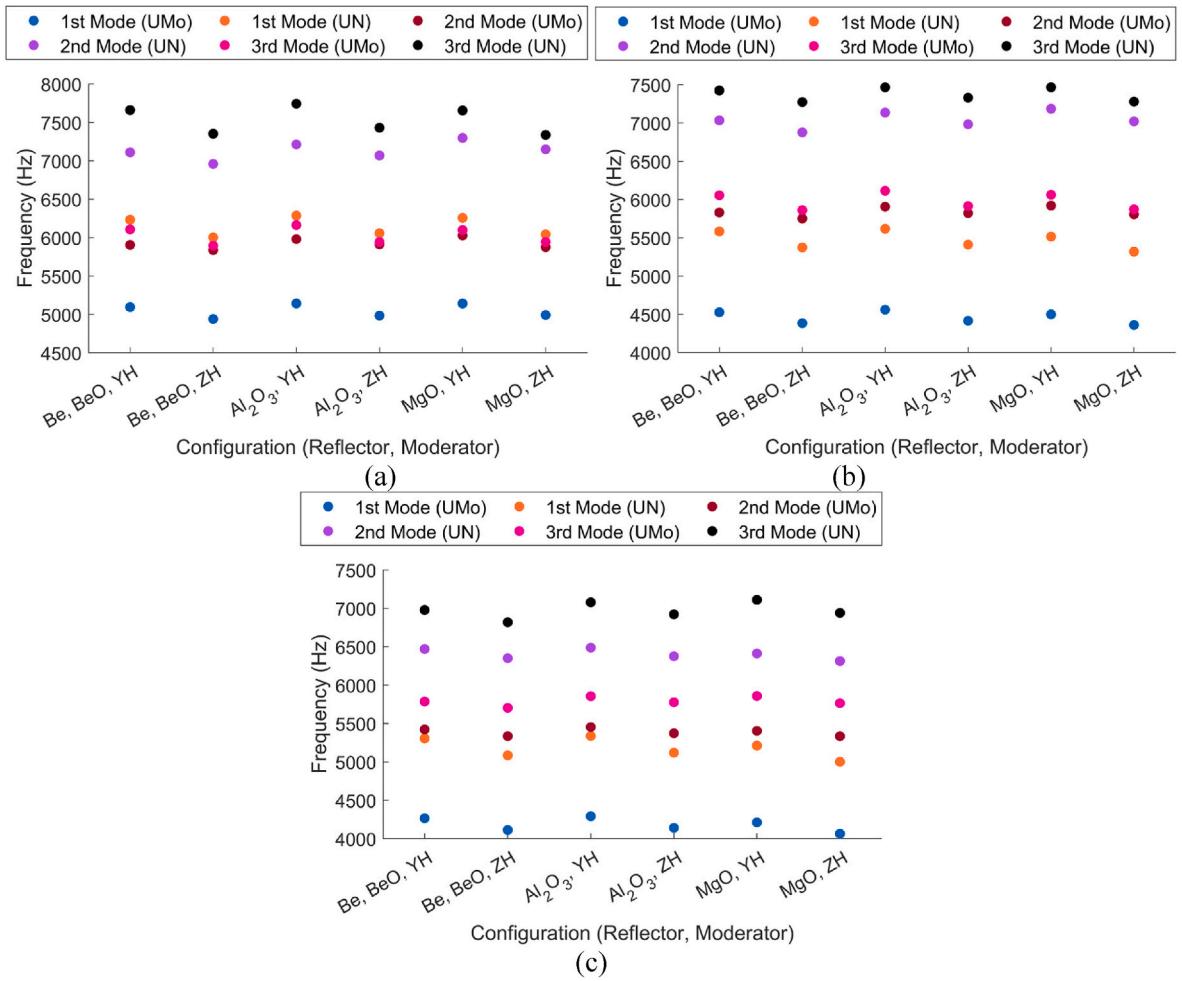

Fig. 14. First three non-symmetric vibration modes for design 3 for boundary conditions: (a) all boundaries fixed (A.B.F), (b) outer bottom fixed (O.B.F), and (c) only outer fixed (O.O.F).

regards to the reflector materials Be, BeO, Al_2O_3, and MgO, their influence on natural frequencies of design is less compared to moderator and fuel materials. This occurs due to more volume occupied by moderator and fuel materials and hence contributing more towards the stiffness of the design. The most influential material parameter for this analysis is the Young's modulus of the reflector and fuel materials, which dictate the change in natural frequencies observed in Fig. 14. From Table 1, we see UN and YH having a higher Young's modulus results in higher natural frequencies of the design, whereas switching to UMo and ZH lowers theses values, respectively. As for UN and UMo, the change is quite significant, since the first three natural frequencies of design 3 with UMo as fuel, are much lower than the second and third natural frequencies of design 3 when UN is selected as fuel material.

From a performance perceptive, mode shapes and natural frequencies should be studied in conjunction to understand which boundary condition and material configuration works best. For design 3, mode shapes do not change with a change in material configuration, but with the change in boundary condition. However, the first mode shape remains the same for all three boundary condition. The second mode shape is a bending mode along the cooling channel for A.B.F and O.B.F conditions. For O.O.F condition, the second mode is a deformation along the cooling channel propagating in opposite direction with nodes present at the middle of the cooling channel. The third mode for all boundaries is a bending mode with a node at the center of the cooling channels. For forced vibration analysis, only the first mode becomes important due to the nature of deformation that can be easily activated during the operation of a micro-reactor.

4.2.2. *Forced vibration analysis with varying boundary conditions*

The forced vibration analysis is simulated based on the results of the eigenfrequency study. The analysis is performed whilst keeping the same twelve material configurations, as discussed in the thermal analysis section. The key parameter in the forced vibration analysis is the damping ratio of the material since it is a property of the material and is the defining property to counteract the effect of vibrations in the system. However, the unavailability of data on damping ratio for our materials digress the authenticity. This can be remedied by keeping this property constant in all of our materials and perform a qualitative analysis of the behavior of stresses and deformations in the system due to forced vibration. The effect of a change in the value of damping ratio is also analyzed. Note that the higher value of the damping ratio used here is likely too high to be found in a realistic material, but it is used here to demonstrate the extreme case. A comparison is made based on the behavior of fuel materials with changing boundary conditions of the system.

Fig. 15 summarizes the cases simulated where the reactor is constrained from all sides and the input amplitude of the applied force per unit area is set to 15 MPa. The frequency of loading matches the first natural frequency of the design and it varies for all configurations. Unlike the study on thermal expansion of micro-reactor, the effect of boundary condition on the location of maximum stresses is not prominent in forced vibrations. For forced vibrations, maximum deformations are found to be nearing the cooling channel for all cases, due to the applied loading at those locations. However, the choice of boundary condition directly affects the natural frequency of design, and hence a

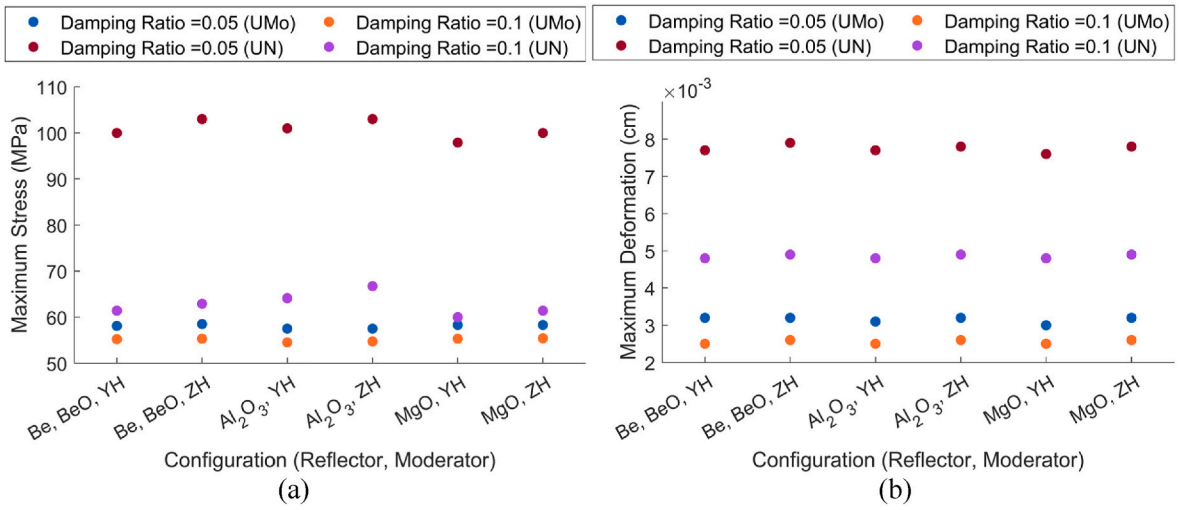

Fig. 15. Maximum von Mises stress (a) and maximum deformation (b) with all boundaries fixed (A.B.F).

change in deformations and stresses are observed. The deformation with UN as fuel material is significantly higher as compared to UMo, for both damping ratios of 0.05 and 0.1. For a damping ratio of 0.05, the maximum stress is observed to reach 105 MPa for the Al_2O_3, ZH, and UN configuration. Simply switching from UN to UMo, brings about a 40 percent reduction in maximum stress. The magnitude for deformation remains similar for all configurations, however, switching from UN to UMo brings a significant decrease in maximum deformation. The highest deformation is calculated for the configurations of Al_2O_3, with Zirconium Hydride as the moderator. The results also point towards Yttrium Hydride as a better moderator compared to Zirconium Hydride, in regards to maximum stresses and maximum deformation in the reactor design.

The A.B.F condition behaves as the exception for the case UMo as fuel, as in other boundary conditions, UMo, as fuel material shows the highest deformation and the resulting stresses, whereas for the case of the A.B.F condition, UMo has less deformation as compared to UN. This behavior is due to the nature of first mode shape for the case UMo with the A.B.F boundary condition, in comparison with UN. The applied loading at the first modal frequency with A.B.F produces a higher deformation UMo in comparison with UN. For the other boundary conditions i.e., O.B.F and O.O.F the first mode of deformation for both UMo and UN are similar and due to the higher elastic modulus of UN deformation is smaller as compared to UMo.

Testing the other two boundary conditions results in an increase in the deformation in the reactor design, compared to the all boundaries fixed condition. The variation in stress and deformation is not found to be signifcant between outer bottom fixed and only outer fixed boundary condition, as seen from Figs. 16 and 17. Only a small reduction in deformation and von Mises stress is seen, when choosing the O.O.F boundary condition over O.B.F boundary. For the case of O.B.F boundary, Be and BeO perform best with both YH and ZH, as the moderator materials, whereas the Aluminum Oxide configurations prove to be the least effective for this design consideration. A switch of fuel material from UMo to UN reduces the stresses even further, which may be beneficial in the long term operation of the design, considering fatigue life and creep stresses.

The mechanical response of the design remained similar with a switch to O.O.F boundary condition. Be and BeO configurations once again prove to be the most effective ones, in terms of minimum deformation and minimum stresses in the design, as shown in Fig. 17. A small decrease in values of both performance parameters is seen with the O.O.F boundary condition. The similarity and minimum change in the results is attributed to a very small drop in the first natural frequency of the design, when the boundary conditions are varied. Similarly, the behavior of Al_2O_3 configuration also remains the same as previous cases, as this configuraiton results in the highest stress with both sets of fuel and moderator materials.

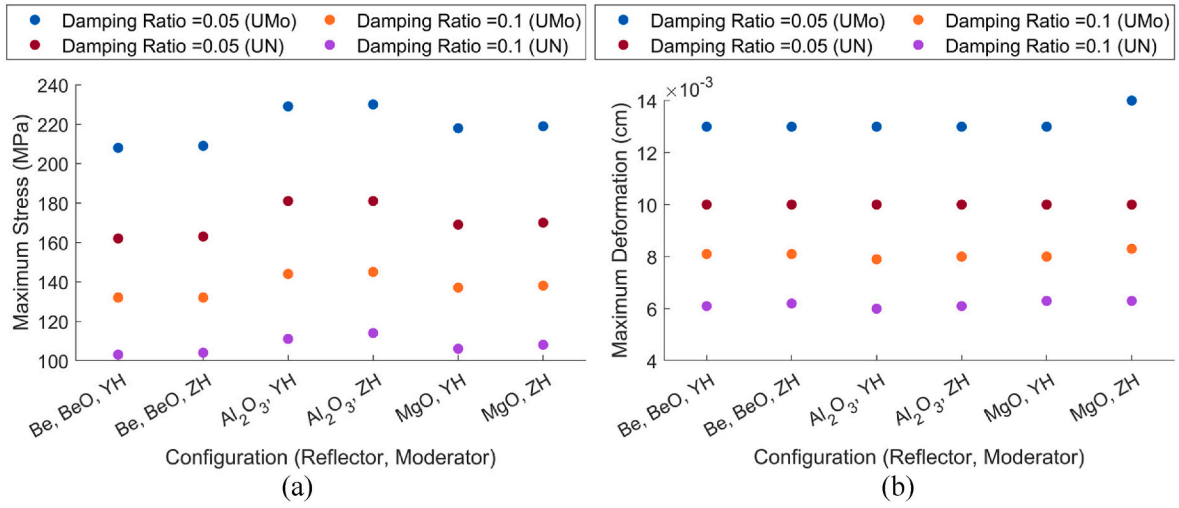

Fig. 16. (a) Maximum von Mises stress and (b) maximum deformation with outer and bottom boundary fixed (O.B.F).

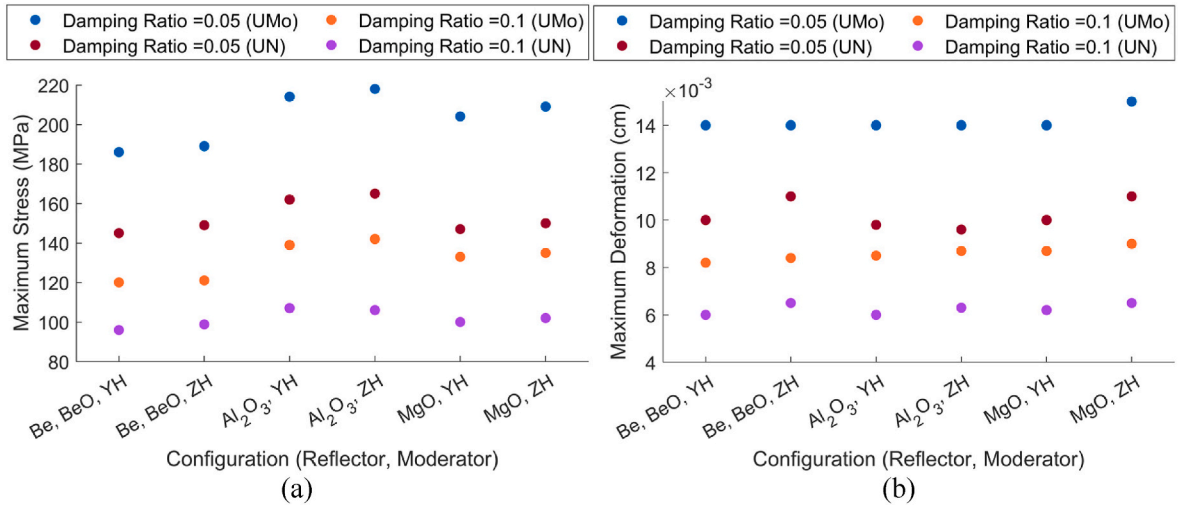

Fig. 17. Maximum von Mises stress (a) and maximum deformation (b) with only outer fixed boundary (O.O.F).

The prime conclusion from this study is the behavior of Aluminum Oxide and Beryllium Oxide as reflector materials. The results points towards Be and BeO to be the most effective as the reactor reflector materials, with Yttrium Hydride being the preferred moderator, purely due to the least amount of maximum deformation and maximum stress generated during reactor operation. A high damping ratio for these materials suggests a significant reduction in stresses, provided significant change in the damping ratio is achieved during the material manufacturing process. The choice of fuel materials remains an open decision depending upon the limits of operation and operating condition. Selecting UMo as the fuel material would result in a small temperature difference in the reactor design, that would be beneficial for the control of hydrogen diffusion during reactor operation. However, this configuration would lead to higher stresses within the system during operation. Similarly, selecting UN as the fuel material will result in an incerased temperature difference in the reactor design, but this choice would lead to a reduced stress distribution and deformation.

5. Conclusions

COMSOL provides an accessible simulation model to accurately predict mechanical and thermal responses of solid structures. This study analyzed the thermal and mechanical profiles of a solid-state microreactor based on the Zebra kW reactor design. The thermal analysis suggested design 3 to be the best in terms of thermal output, as results show minimum temperature difference and low deformation due to the thermal expansion of materials. For this design, the only outer fixed boundary is optimal as it results in the low stress generation in the reactor design, whilst considering results of forced vibration. For thermal analysis, it is found that boundary conditions do not play a significant role towards a change in stresses, since a minor change is observed whilst switching between boundary conditions. However, O.O.F boundary condition proves to be a better option for that case, as the results showed the least amount of stresses in design 3 with that selection. In terms of materials, Beryllium and Beryllium Oxide perform best as reflector materials when paired with Yttrium Hydride as the moderator. The selection of fuel material between Uranium Molybdenum and Uranium Nitride remains an open question, as they correspond to maximum permissible stress and maximum permissible temperature difference in the reactor. Future investigations can be carried out by examining the effects of crack propagation and fatigue failure in combination with mechanical and thermal loading to obtain a clearer understanding of the system and its performance.

CRediT authorship contribution statement

M. Anjum: Writing – original draft, Visualization, Software, Methodology, Investigation, Formal analysis, Data curation. **T. Gibson:** Writing – review & editing, Visualization, Supervision, Methodology, Funding acquisition, Formal analysis, Conceptualization. **G.T. Craven:** Writing – review & editing, Visualization, Supervision, Methodology, Funding acquisition, Formal analysis, Conceptualization. **S. Tretiak:** Writing – review & editing, Visualization, Supervision, Methodology, Funding acquisition, Formal analysis, Conceptualization. **A. Abdelkefi:** Writing – review & editing, Visualization, Supervision, Resources, Project administration, Methodology, Investigation, Funding acquisition, Formal analysis, Conceptualization.

Declaration of competing interest

The authors declare that they have no known competing financial interests or personal relationships that could have appeared to influence the work reported in this paper.

Data availability

Data will be made available on request.

Acknowledgements

The authors M. Anjum and A. Abdelkefi acknowledge the financial support from Los Alamos National Laboratory. Research presented in this article was supported by the Laboratory Directed Research and Development program of Los Alamos National Laboratory under project number 20220053DR. The research is performed in part at the Center for Integrated Nanotechnologies (CINT), a U.S. Department of Energy, Office of Science user facility at LANL. LANL is operated by Triad National Security, LLC, for the National Nuclear Security Administration of the U.S. Department of Energy under Contract No. 89233218CNA000001.

References

Amestoy, P.R., Duff, I.S., L'excellent, J.Y., 2000. Multifrontal parallel distributed symmetric and unsymmetric solvers. Comput. Methods Appl. Mech. Eng. 184 (2–4), 501–520.
Araki, D., Kurosaki, K., Kimura, H., Muta, H., Ohishi, Y., Konashi, K., Yamanaka, S., 2015. Thermal and mechanical properties of hydrides of Zr–Hf alloys. Journal of Nuclear Science Technology 52 (2), 162–170.
AZoM Magnesia - Magnesium Oxide (MgO) Properties & Applications, 2023.
Bauccio, M., 1994. ASM Engineering Materials Reference Book.

Black, G., Shropshire, D., Araújo, K., van Heek, A., 2023. Prospects for nuclear micro-reactors: a review of the technology, economics, and regulatory considerations. Nucl. Technol. 209 (Suppl. 1), S1–S20.
Bobkov, V., Fokin, L., Petrov, E., Popov, V., Rumiantsev, V., Savvatimsky, A., 2008. Thermophysical Properties of Materials for Nuclear Engineering: a Tutorial and Collection of Data. IAEA, Vienna.
Carlson, L., Miller, J., Wu, Z., 2022. Implications of HALEU fuel on the design of SMRs and micro-reactors. Nucl. Eng. Des. 389, 111648.
COMSOL. The PARDISO Solver. Available from: https://doc.comsol.com/5.5/doc/com.comsol.help.comsol/comsol_ref_solver.27.118.html.
Dorogokupets, P., Sokolova, T.S., Dymshits, A.M., Litasov, K.D., 2016. Thermodynamic properties of rock-forming oxides, α-Al2O3, Cr2O3, α-Fe2O3, and Fe3O4 at high temperatures and pressures. ГеодинаМика и тектонофизика 7 (3), 459–476.
Fan, T., Zhang, Y., Yang, G., Song, Y., Jiang, J., 2023. Transport vibration analysis of mobile liquid Pb-Bi micro-reactors with non-uniform mass distribution. Nucl. Eng. Des. 414, 112612.
Gabbar, H.A., Abdussami, M.R., Adham, M.I., 2020. Micro nuclear reactors: potential replacements for diesel gensets within micro energy grids. Energies 13 (19), 5172.
Hu, G., Hu, G., Hu, R., Kelly, J.M., Ortensi, J., 2019. Multi-physics Simulations of Heat Pipe Micro Reactor. Argonne National Lab.(ANL), Argonne, IL (United States).
Hu, X., Wang, H., Linton, K., Le Coq, A., Terrani, K.A., 2021. Handbook On the Material Properties Of Yttrium Hydride For High Temperature Moderator Applications. Oak Ridge National Lab.(ORNL), Oak Ridge, TN (United States).
Im, J., Jeong, M.J., Choi, N., Kim, K.M., Cho, H.K., Joo, H.G., 2023. Multiphysics analysis system for heat pipe cooled micro reactors employing PRAGMA-OpenFOAM-ANLHTP. Nucl. Sci. Eng. 1–15.
Konings, R., Stoller, R.E., 2020. Comprehensive Nuclear Materials. Elsevier.
Marcum, W.R., Nixon, C.A., Martin, M., Steer, K.M., Jackson, R.B., Weiss, A.W., 2023. Flow induced vibration measurement of a full-length sodium fast reactor fuel bundle. Nucl. Eng. Des. 408, 112322.
Matthews, C., Laboure, V., DeHart, M., Hansel, J., Andrs, D., Wang, Y., Ortensi, J., Martineau, R.C., 2021. Coupled multiphysics simulations of heat pipe micro-reactors using DireWolf. Nucl. Technol. 207 (7), 1142–1162.
McClure, P.R., Poston, D.I., Gibson, M.A., Mason, L.S., Robinson, R.C., 2020. Kilopower project: the KRUSTY fission power experiment and potential missions. Nucl. Technol. 206 (Suppl. 1), S1–S12.
Mehta, V.K., Rao, D.V., 2022. Suppressing the positive temperature reactivity coefficient in metal hydride moderated reactor. In: Proceedings of the International Conference on Physics of Reactors-PHYSOR 2022.
Mehta, V.K., McClure, P., Kotlyar, D., 2019. Hydrogen loss effects on micro-reactors for space and planetary nuclear power production. In: AIAA Propulsion and Energy 2019 Forum.
Mehta, V.K., Shivprasad, A.P., Rao, D.V., 2024. Startup and multiphysics analysis of a compact kW-class thermal spectrum micro-reactor. Nucl. Technol. 1–19.
Phillips, A., Mickum, G., Burkes, D., 2010. Thermophysical Properties of U-10MO Alloy. Idaho National Lab.(INL), Idaho Falls, ID (United States).
Rao, D.V., Trellue, H., Arafat, M.Y., 2020. Micro-reactors: A Technology Option for Accelerated Innovation. Los Alamos National Lab.(LANL), Los Alamos, NM (United States); Idaho.
Sabharwall, P., Hartvigsen, L., Morton, J., Yoo, J., Qin, Su, Song, M., Guillen, D., Unruh, T., Hansel, J., Jackson, J., 2023. Nonnuclear experimental capabilities to support design, development, and demonstration of micro-reactors. Nucl. Technol. 209 (Suppl. 1), S41–S59.
Schenk, O., Gärtner, K., 2004. Solving unsymmetric sparse systems of linear equations with PARDISO. Future Generat. Comput. Syst. 20 (3), 475–487.
Stauff, N.E., Abdelhameed, A., Cao, Y., Kristina, N., Miao, Y., Mo, K., Nunez, D., 2022. Multiphysics Analysis of Load Following and Safety Transients for Micro-reactors. Argonne National Laboratory (ANL), Argonne, IL (United States). Idaho National Laboratory (INL), Idaho Falls, ID (United States).
Sun, X., Chai, G., Bao, Y., 2017. Elastic and elastoplastic fracture analysis of a reactor pressure vessel under pressurized thermal shock loading. Eur. J. Mech. Solid. 66, 69–78.
Taylor, K.M., McMurtry, C.H., 1961. Synthesis and Fabrication of Refractory Uranium Compounds. Summary Report for May 1959 through December 1960. Carborundum Co. Research and Development Div., Niagara Falls, NY.
Testoni, R., Bersano, A., Segantin, S., 2021. Review of nuclear micro-reactors: status, potentialities and challenges. Prog. Nucl. Energy 138, 103822.
Vogel, S.C., Monreal, M.J., Shivprasad, A.P., 2021. Materials for small nuclear reactors and micro reactors, including space reactors. JOM 73, 3497–3498.
Xiao, W., Li, X., Li, P., Zhang, T., Liu, X., 2022. High-fidelity multi-physics coupling study on advanced heat pipe reactor. Comput. Phys. Commun. 270, 108152.
Yamanaka, S., Yoshioka, K., Uno, M., Katsura, M., Anada, H., Matsuda, T., Kobayashi, S., 1999. Thermal and mechanical properties of zirconium hydride. J. Alloys Compd. 293, 23–29.
Zhou, Y., Wang, J., Guo, Z., He, Y., Zhang, Y., Qiu, S., Su, G.H., Corradini, M.L., 2021. 3D-2D coupling multi-dimension simulation for the heat pipe micro-reactor by MOOSE&SAM. Prog. Nucl. Energy 138, 103790.
Zohuri, B., 2021. Nuclear micro power reactor: the new generation of innovative small reactors. Modern Approaches on Material Science 4, 530–533. https://doi.org/10.32474/MAMS.2021.04.000189.